Optical breakdown in aluminum vapor induced by ultraviolet laser radiation

V. I. Mazhukin, V. V. Nossov, and M. G. Nickiforov
Institute of Mathematical Modeling of RAS, 4a Miusskaya sqr., 125047 Moscow, Russia

I. Smurov[a)]
Ecole Nationale d'Ingénieurs de Saint-Etienne, 58 rue Jean Parot, 42023 Saint-Etienne Cedex 2, France

(Received 24 July 2002; accepted 30 September 2002)

Theoretical analysis of the evolution of nonequilibrium plasma induced by ultraviolet laser radiation is carried out. Intensity threshold values are studied by mathematical modeling as a function of laser-pulse wavelength. Basic mechanisms of nonequilibrium ionization of aluminum vapor are analyzed and the dominant role of photo-processes, namely, resonant and nonresonant photoexcitation and photoionization, is shown. The modeling results are in good agreement with experimental data on optical breakdown in aluminum vapor by the excimer laser radiation in nanosecond and microsecond range. © *2003 American Institute of Physics.*
[DOI: 10.1063/1.1522810]

I. INTRODUCTION

A powerful laser radiation flux focused at the target surface causes its evaporation, optical breakdown, and development of a plasma in the evaporated material. The appearance of the plasma near irradiated surfaces of solid bodies changes qualitatively the character of thermal and mechanical influence of powerful laser radiation on the target. Therefore, determining the threshold conditions of evaporation and plasma formation is an important task for numerous laser applications. On the other hand, the development and promising applications of high-power excimer lasers (e.g., pulsed laser deposition[1,2] and laser shock processing technologies[3,4]) has given the priority to investigations of the ultraviolet (UV) *range* of laser action.

The process of pulsed laser evaporation accompanied by plasma formation in the evaporated material is a complex and manifold phenomenon. It can only be described within the framework of a so-called conjugate approach that simultaneously takes into consideration the processes of nonequilibrium heating and ionization in condensed and gaseous media. In view of the complexity of the problem, it is expedient to separately investigate its constituent aspects.

The present work considers only the initial stage of plasma formation–optical breakdown in aluminum vapor-induced by UV laser radiation with the wavelength λ_1 ranging from 0.4 to 0.1 μm. The choice of the initial stage of plasma formation as a subject of the investigation is governed by the following reasons. Optical breakdown is a nonequilibrium process of transition of the medium from the stage of a partially ionized gas transparent for laser radiation, in which $\nu_{en} \gg \nu_{ei}$, into an opaque for laser radiation plasma, where the inverse relation is fulfilled $\nu_{en} \ll \nu_{ei}$. Here, ν_{en}, ν_{ei} are the frequencies of electron-neutral and electron-ion interactions. To describe this process, it is sufficient to apply the appropriate kinetic collision-radiation model supplemented by the energy balance equations.[5,6] In a medium, that is initially at rest, the radiation transfer and the macroscopic movement of vapor start much later, when the system approaches the state of local thermodynamic equilibrium, therefore, at the initial stage of breakdown they can be neglected. Thus, mathematical formulation of the problem gets simpler, while the threshold conditions of plasma formation and its characteristic duration can be determined with sufficient accuracy.

The investigation of the mechanisms of optical breakdown in metal vapors, as well as the interaction and changes of these mechanisms, makes it necessary to analyze the kinetics of multilevel systems populating that can be quantitatively described by appropriate kinetic models. Note that the collision-radiation models[5,6] that have earlier been applied for modeling optical breakdown of metal vapors of Al and Cu by the action of CO_2 and yttrium aluminum garnet (YAG)-lasers cannot now be used for similar purposes in the case of the excimer laser. As it was noted before, in the infrared (IR) range, the main mechanism of electromagnetic field energy dissipation is the inverse-bremsstrahlung effect whose cross section changes with growing frequency as ω^{-3}.[7] This means that in the UV range, the efficient heating of the electrons will be diminished sharply. Consequently, in the UV range, the breakdown must be achieved by a considerable increase of the threshold intensity G^*. According to the classical theory, the frequency dependence of the threshold intensity has the form $G^* \sim \omega_l^2$.[7] At the same time, numerous experiments[8–20] point to the opposite. In the UV range, the threshold intensity has been found not to increase but to decrease. In pure gases, the classical dependence $G^* \sim \omega_l^2$ is satisfied up to the frequencies corresponding to that of the ruby laser $\omega_l \approx 5 \times 10^{14}$ s^{-1}.[8] The main peculiarities of the interaction of radiation with a vapor in the UV range are attributed to the fact that the value of the quantum becomes comparable to the excitation energy of the electron states and the potential of their ionization. An important role of the photoionization process in optical breakdown in metal vapors induced by 0.35 μm laser radiation has been confirmed by calculations.[11,21] However, in those works, photoexcita-

[a)]Electronic mail: smurov@enise.fr.

tion processes were neglected. The results of the present work revealed that in the excimer laser radiation–vapor interaction, an important role is played by the processes of nonresonant photoexcitation and photoionization of atoms and ions by the laser radiation.

At present there exists extensive experimental information on optical breakdown in gaseous media induced by the laser radiation in the UV range. However, interpretation of some experimental results on interaction of UV radiation is quite difficult because of a complex nonequilibrium character of the processes as a whole. Moreover, most available experimental data have been obtained using different criteria of plasma formation that are not only different from one another but also from theoretical estimations.[22] In our article, we attempt to analyze, from a general point of view, the kinetics of UV laser-induced optical breakdown in Al vapor, and compare the theoretical predictions for plasma formation thresholds to experimental data.

From the theoretical point of view, the principal purpose of the work is to develop a nonequilibrium kinetic model for a multilevel system that is typical for atoms and ions of metals, taking into consideration not only collision-radiation transitions but also the main photoionization-recombination processes. Simultaneous consideration of the energy balance of two subsystems—the electronic and atomic-ionic ones—makes it possible to apply it for the description of optical breakdown in a wide frequency range $\hbar\omega_l \in [0.1-10]$ eV that approximately corresponds to the radiation range of modern lasers ranging from the CO_2 laser to the ArF excimer laser. The developed kinetic model was used to model several interaction regimes close to experimental situations[9–11] in which optical breakdown in aluminum vapor by the excimer laser radiation was investigated.

II. STATEMENT OF THE PROBLEM

The laser radiation of the intensity $G=G_0\times f(t)$ with the wavelength λ_l and the temporal form $f(t)$ directed to a thin layer of an evaporated material with the temperature T_0 and the density ρ_0. If the maximum radiation intensity G_0 is smaller than a certain threshold value G^*, the evaporated substance turns out to be optically transparent and the laser radiation passes through the system under consideration practically with no absorption. At $G_0>G^*$, the optical thickness of the layer turns out to be sufficient for the initial laser radiation to be absorbed. The laser radiation absorption leads to an additional heating of the medium and to an increase of its optical density, which ultimately results in an avalanche ionization of the evaporated material. At the moment of optical breakdown, the collision frequencies are approximately equal $\upsilon_{en}\approx\upsilon_{ei}$.[5,23] The dynamics of the process depends on both the characteristics of the evaporated material (its temperature, density, electron configuration, transition energy, and the ionization potential of atoms) and the laser action mode (the intensity, the wavelength, the duration, and the pulse temporal shape).

The vapor is assumed to be initially in an equilibrium state. The corresponding initial concentrations of electrons and ions in the ground and excited states can be found from the Saha–Boltzmann equations. The initial values of the temperature T_0 and the density ρ_0 of the vapor correspond to the parameters of the onset of intensive evaporation of the metal under normal conditions: $T_0=T_b$, $\rho_0=\rho(T_0)$, where T_b is the equilibrium boiling temperature. The medium with T_0 and ρ_0 defined in this way corresponds to the state of a partially ionized gas with a moderate ionization $\alpha=N_e/N_0 \ll 1\approx(10^{-5}-10^{-4})$. At a later time, at a sufficient laser radiation intensity and as a result of the inverse-bremsstrahlung effect or photoionization heating of free electrons in a metal vapor, conditions adequate for initiating an avalanche ionization, i.e., optical breakdown can be realized.

A. Transient collision-radiation model

In an evaporated matter (the vapor) interacting with laser radiation, a great number of elementary reactions take place. The total of them determines the character of the macroprocess. Mathematical models describing the level–by–level kinetics, photoprocesses and ionization-recombination processes are based on the electron configuration of atoms and ions under study.[5] Considerations of the threshold conditions of plasma formation showed that the characteristic temperature of the electron gas does not usually exceed a few electron volts. Therefore it is sufficient to restrict a mathematical description of optical breakdown by the account of kinetic processes for the case of a neutral atom with the ionization potential $J_0=5.986$ eV. Table I represents the principal elementary processes that are taken into account in the collision-radiation model as well as the expressions for the reaction rates. A sketch of the processes is shown in Fig. 1.

B. System of equations

The concentration of charged particles (ions N_i and electrons N_e, N_e, N_i) and the population of excited levels in neutral atoms N_n are described by the following system of nonlinear differential equations:

$$\frac{dN_0}{dt}=-\sum_{m=1}^{M}(k_{0m}N_0-r_{m0}N_m)N_e - (\alpha_0 N_0-\beta_0 N_i N_e)N_e+\sum_{m=1}^{M}A_{m0}N_m-\sum_{m=1}^{M}\upsilon_{0m}^{c}\times\left(N_0-\frac{g_0}{g_m}N_m\right)-\sum_{m=1}^{M}\upsilon_{0m}^{l}\left(N_0-\frac{g_0}{g_m}N_m\right) - (\upsilon_0^l+\upsilon_0^c)N_0+(R_0^c+R_0^l)N_i N_e, \quad (1)$$

$$\frac{dN_n}{dt}=\sum_{m=0}^{n-1}(k_{mn}N_m-r_{nm}N_n)N_e-\sum_{m=n+1}^{M}\times(k_{nm}N_n-r_{mn}N_m)N_e-(\alpha_n N_n-\beta_n N_i N_e)N_e+\sum_{0\le m<n}\upsilon_{mn}^{l}\left(N_m-\frac{g_m}{g_n}N_n\right)-\sum_{n<m\le M}\upsilon_{nm}^{l}\left(N_n-\frac{g_n}{g_m}N_m\right)+\sum_{0\le m<n}\upsilon_{mn}^{c}\left(N_m-\frac{g_m}{g_n}N_n\right)$$

TABLE I. The elementary processes included into the model. In the case of the values having double subscripts, the first subscript denotes the number of the initial transition state and the second subscript denotes the number of the final transition state; z is the charge of ion, $z=1$; ξ_n is the quantity of equivalent electrons in the n-th state; $S_{mn}(\Delta\omega)$ is the spectral function of the Voigt profile of the line characterizing the dependence of the laser excitation reaction rate on the amount of the discrepancy between the laser frequency ω_l and the transition frequency ω^0_{mn}. $S_{mn}(\Delta\omega)$ is calculated as a convolution of the Doppler $S^D_{mn}(\Delta\omega)$ contour and the Lorentz $S^L_{mn}(\Delta\omega)$ contour (see Ref. 25).

Reaction name *Reaction type*	*Notation*	*Rate coefficient*	Ref.
1. Spontaneous decay			
$Al_m \rightarrow Al_n + \hbar\omega_{mn}$	A_{mn} [s^{-1}]	$A_{mn}=8\times10^5\{\Delta E_{mn}/\mathrm{Ry}\}^2 g_m/g_n f_{mn}$	24, 25
2. Collisional excitation/deexcitation			
$Al_m + e \leftrightarrow Al_n + e$	k_{mn}, r_{nm} [$cm^3\times s^{-1}$]	$k_{mn}=1.58\times10^5 f_{mn}/(\Delta E_{mn}T_e^{0.5})\exp\{\Delta E_{mn}/T_e\}Q_{mn}$ $Q_{mn}=A+Cx_{mn}+[Bx_{mn}-C(x_{mn})^2$ $+D]\exp\{\Delta E_{mn}/T_e\}Ei(x_{mn})$ $r_{nm}=k_{mn}g_n/g_m\exp(-x_{nm}),\quad x_{mn}=\Delta E_{mn}/T_e$	26, 27
3. Collisional ionization			
$Al_m + e \rightarrow Al_i + 2e$	α_m [$cm^3\times s$]	$\alpha_m=3.14\times10^{-6}[\xi_m Ei(x_m)]/(T_e^{3/2}x_m)\exp(-x_m)$	28, 29
4. Three-particle recombination			
$Al_i + 2e \rightarrow Al_m + e$	β_m [$cm^6\times s$]	$\beta_m=\alpha_m\times\frac{g_m}{g_e g_0}\left\{\frac{2\pi\hbar^2}{mT_e}\right\}^{3/2}\exp(x_m)$	7
5. Laser-induced photoionization			
$Al_m + \hbar\omega_l \rightarrow Al_i$	v^l_m [s^{-1}]	$v^l_m=\left(\frac{G}{\hbar\omega_\ell}\right)\times\sigma_m(\hbar\omega_\ell),\quad \sigma_m=7.8\times10^{-18}\frac{m}{z^2}\left(\frac{J_m}{\hbar\omega_\ell}\right)^3$	30, 31
6. Continuous radiation-induced photoionization			
$Al_m + \hbar\omega_c \rightarrow Al_i$	v^c_m [s^{-1}]	$v^c_m=3.5\times10^7 z^4\int_{2.8x}^{\infty}\frac{dy}{y[\exp(y)-1]}\Big/\int_{2.8}^{\infty}\frac{dy}{y[\exp(y)-1]}$ $x=z^2\mathrm{Ry}/2.8T_e$	32
7. Laser-induced photorecombination			
$Al_i + e + \hbar\omega_l \rightarrow Al_m + \hbar\omega_l$	R^l_m [$cm^3\,s^{-1}$]	$R^\ell_m=10^{-3}g_m T_e^{-3/2}\sigma_m(\hbar\omega_l)\left(\frac{G}{\hbar\omega_l}\right)\exp\left(\frac{J_m-\hbar\omega_l}{T_e}\right),$ $J_m\leqslant\hbar\omega_\ell,\quad J_m=J_0-E_m$	33
8. Continuous radiation-induced photorecombination			
$Al_i + e + \hbar\omega_c \rightarrow Al_m + \hbar\omega_c$	R^c_m [$cm^3\,s^{-1}$]	$R^c_m=5.2\times10^{-14}z(J_m/T_e)^{3/2}\exp(x_m)E_1(x_m)\xi_m/2m^2,$ $E_1(x_m)=\exp(-x_m)\left(\ln\frac{1+x_m}{x_m}-\frac{0.4}{(1+x_m)^2}\right),\quad x_m=\frac{J_m}{T_e}$	7
9. Laser-induced photoexcitation			
$Al_m + \hbar\omega_l \rightarrow Al_n$	v^l_{mn} [s^{-1}]	$v^\ell_{mn}=\left(\frac{\pi c}{\omega_{mn}}\right)^2\frac{g_n}{g_m}\frac{G}{\hbar\omega}A_{mn}S_{mn}(\Delta\omega),\quad \Delta\omega=\omega_l-\omega^0_{mn},\omega^0_{mn}=\frac{E_{mn}}{\hbar},$	25, 34
		$S_{mn}(\Delta\omega)=\int_{-\infty}^{\infty}S^L_{mn}(\Delta\omega)S^D_{mn}(\Delta\omega)dy$ $=\frac{a}{\pi^{3/2}\gamma_D}\int_{-\infty}^{\infty}\frac{\exp(-y)^2}{a^2+[(\Delta\omega/\gamma_D)-y]^2},$	35
		$a=\frac{\Delta\omega_L}{\Delta\omega_D},\ \Delta\omega_D=\frac{\omega}{c}\sqrt{\frac{2T_g}{M_g}},\quad \Delta\omega_L=\Delta\omega_{ei}+\Delta\omega_{ai},$	
		$\Delta\omega_{ei}=\frac{32}{3}\frac{C_2^2}{V_e}\left(2.556-\ln\frac{2C_2^2}{\rho_D.V_e}\right)N_i,\quad x=\frac{13.6z^2}{J_0,-E_m}$	32, 36
		$\rho_D=[T_g/4\pi e^2(N_e+N_i)]^{0.5},\quad C_2=0.869zm(m+1)$	37
		$\Delta\omega_{ai}=17\times C_6^{0.4}V_g^{0.6}N_0,\ C_6=6.46\times10^{-34}\Delta r^{-2},$	
		$\Delta r^{-2}=\frac{x(5x+1)}{2z^2},$	38
10. Continuous spectrum photoexcitation			
$Al_m + \hbar\omega_c \rightarrow Al_n$	v^c_{mn} [s^{-1}]	$v^c_{mn}=\left(\frac{\pi c}{\omega_{mn}}\right)^2\frac{g_n}{g_m}\frac{I_{b\omega}}{\hbar\omega_c},\quad I_{b\omega}=\frac{\hbar\omega_c}{4c^2\pi^3[\exp(\hbar\omega_c/T_e)-1]}$	39

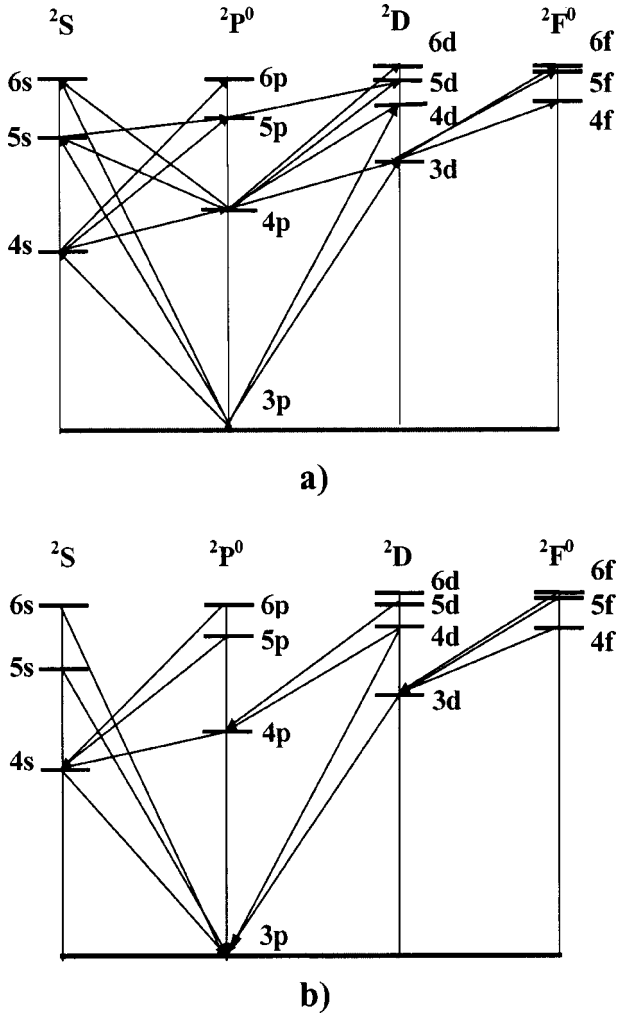

FIG. 1. Energy scheme of collision (a) and radiation (b) transitions of the aluminum atom.

$$-\sum_{n<m\leq M} v_{nm}^{c}\left(N_n-\frac{g_n}{g_m}N_m\right)-\sum_{0\leq m<n} A_{nm}N_n+\sum_{n<m\leq M} A_{mn}N_m+(R_n^c+R_n^l)N_iN_e-(v_n^c+v_n^l)N_n \quad n=1,2,...,M, \tag{2}$$

$$\frac{dN_i}{dt}=\frac{dN_e}{dt}=\sum_{n=0}^{M}(\alpha_nN_n-\beta_nN_iN_e)N_e+\sum_{n=0}^{M}[(v_n^c+v_n^l)N_n-(R_n^c+R_n^l)N_iN_e], \tag{3}$$

where Eq. (1) describes the ground state of neutral atoms; Eq. (2) describes the population of the excited states of the atom; and Eq. (3) describes the density of the charged particles.

The energy balance of a nonequilibrium plasma is characterized by two temperatures: The electron temperature T_e and the atomic-ionic temperature T_g. The energy balance equations for translational degrees of freedom for electrons and heavy particles are written in the following way:

$$\frac{3}{2}\frac{d}{dt}(N_eT_e)=\left\{[\mu G-\tfrac{3}{2}\delta(T_e-T_g)](v_{en}+v_{ei})-\sum_{n=0}^{M}Q_{n,J}-\sum_{n=0}^{M-1}Q_{n,\Delta E}\right\}N_e+\sum_{n=0}^{M-1}Q_{n,\Phi}, \tag{4}$$

$$\frac{3}{2}\frac{d}{dt}(N_gT_g)=\frac{3}{2}\delta(T_e-T_g)(v_{en}+v_{ei})N_e, \tag{5}$$

$$\mu=\frac{4\pi e^2}{m_ec(\omega^2+(v_{en}+v_{ei})^2)},\quad \delta=\frac{2m_e}{M_g},$$

$$N_g=\sum_{n=0}^{M}N_n+N_i,$$

$$Q_{n,\Delta E}=\sum_{m=n+1}^{M}\Delta E_{nm}(k_{nm}N_n-r_{mn}N_m),$$

$$Q_{n,J}=J_n(\alpha_nN_n-\beta_nN_iN_e),$$

$$Q_{n,\Phi}=(\hbar\omega_l-J_n)(v_n^lN_n+R_n^lN_eN_i)+(\hbar\omega_c-J_n)\times(v_n^cN_n+R_n^cN_eN_i),$$

where $Q_{n,\Delta E}$, $Q_{n,J}$, and $Q_{n,\Phi}$ are the specific powers characterizing the energy exchange due to inelastic collisions, ionization-recombination, and photoionization–photorecombination, respectively; E_n is the excitation energy of the n-th level of the atom, J_0, J_n are the ionization energies of the ground and n-th states, respectively, m_e, M_g are the mass of the electron and heavy particle (atom or ion).

The system of differential Eqs. (1)–(5) is supplemented by the corresponding initial conditions

$$t=0:\ N_0(0)=N_0^0;\quad N_n(0)=N_n^0,\quad n=1,...,M;$$

$$N_i(0)=N_e(0)=N_e^0;\quad T_e(0)=T_g(0)=T_o. \tag{6}$$

Thus, the equations for the population of the energy levels and the charge composition (1)–(3) together with energy balance Eqs. (4) and (5) and the initial conditions (6) form a correct differential problem that describes the dynamics of the processes in a nonequilibrium laser-induced spatially uniform plasma.

The system of nonlinear differential Eqs. (1)–(5) is referred to as a stiff system, i.e., a system whose solution contains both fast and slowly varying components. Solving stiff systems by numerical methods is known to be difficult.[40,41] To date, the theoretical foundations for the methods of solving similar systems of great dimensionality,[42] including those with a varying degree of stiffness,[43] have been adequately developed. In practice, they have been realized in the form of various software.[44,45,46]

To solve the system of Eqs. (1)–(5), one modification of the Gear–Adams method was used, this modification belonging to the family of multistep methods of the predictor-corrector type. Just as in Ref. 46, the software provides pos-

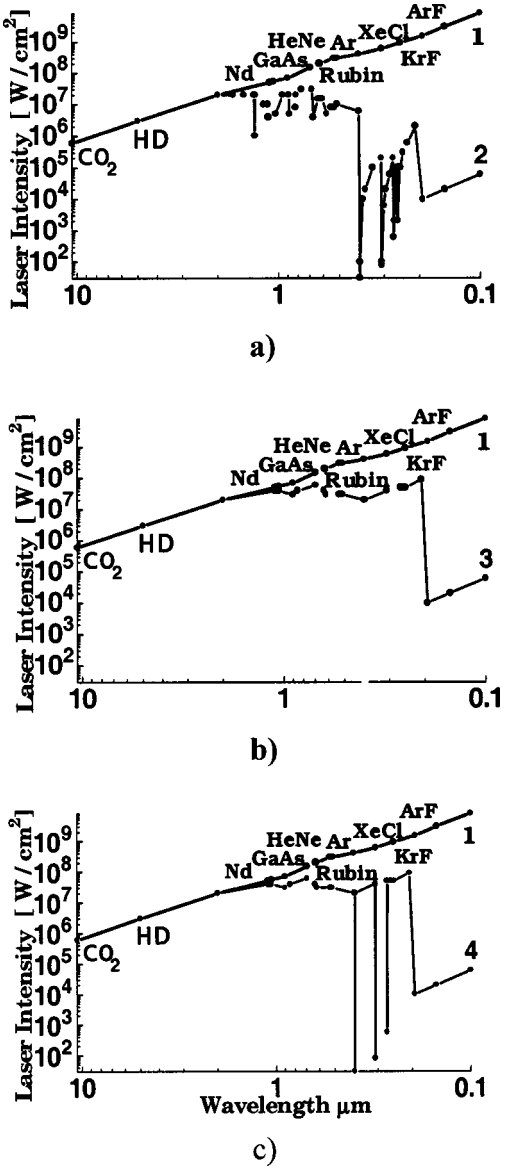

FIG. 2. Wavelength dependence of threshold intensity $G^*(\omega)$ with allowance for (a) all the photoprocesses, (b) photoionization, and (c) resonance photoexcitation.

sibilities to choose automatically an integration step and to switch from Gear's stiff method to Adam's nonstiff one.

C. Saha–Boltzmann equations

To determine equilibrium values of the concentrations of ions N_0^{Saha} and electrons N_e^{Saha}, the nonlinear system of Saha equations was used.[7] Equilibrium concentrations were calculated for two temperatures $T_k=T_e$ and $T_k=T_g$, then the values obtained were compared with similar values derived from the solution of kinetics Eqs. (1)–(5)

$$\frac{N_e^{\mathrm{Saha}}(T_k)\sum_{n=0}^{M}[N_n^{\mathrm{Saha}}(T_k)]}{\sum_{n=0}^{M}[N_n^{\mathrm{Saha}}(T_k)]}=\frac{g_e g_i}{g_0}\left\{\frac{m_e T_k}{2\pi\hbar^2}\right\}^{3/2}\exp\left(\frac{J_0}{T_k}\right)T_k \in\{T_e,T_g\}. \tag{7}$$

The populations of the excited levels were estimated from the population of the ground-state N_0, using the known Boltzmann relation

$$N_n=N_0\frac{g_n}{g_0}\exp\left(-\frac{\Delta E_{0n}}{kT_k}\right), \tag{8}$$

where g_e, g_i are the statistical weights of the electrons and ions and g_n is the statistical weight of the state n.

III. ANALYSIS OF SIMULATION RESULTS

In investigations, the initial state of a metal vapor was simulated by giving the initial values of the temperature T_0 and the density ρ_0 that were close to those on the outside of the Knudsen layer[47] corresponding to the process of evaporation in a vacuum, with the temperature of the aluminum surface being equal to the equilibrium boiling temperature under normal conditions ($T_b=2720$, K$=0.234$ eV, $p=1$ bar): $T_0=0.67T_b$, $\rho_0=\rho_s(T_b)$, where $\rho_s(T_b)$ is the density of saturated vapor. It was assumed that at the initial instant of the time $t=0$, the substance was at the state of thermodynamical equilibrium that corresponds to the Boltzmann population of excited levels (8), the Maxwell distribution of electrons in energy, and the charge composition obeying the Saha relations (7). These conditions correspond to the following values: $T_0=0.2$ eV, $N_0^0=\rho_0/M_A=6\times10^{18}$ cm^{-3}, and $N_e^0=3\times10^{14}$ cm^{-3}.

Summarizing experimental and theoretical data of Refs. 8–22 on optical breakdown in metal vapors, it should be notified that the main peculiarities of the process depend on the following parameters: The radiation intensity G, the wavelength λ_ℓ, the action duration τ_ℓ, and the pulse temporal shape $f_\ell(t)$. In order to reduce the number of parameters, first of all, the action duration τ_ℓ and the pulse temporal shape $f_\ell(t)$ should be excluded from consideration. For this purpose, let us consider the action of a rectangular pulse with a duration that is unlimited in time. Unlimited duration implies that a pulse duration is much longer than a characteristic time taken for a breakdown to occur, for example, $\tau_\ell=(10^{-3}-1)$s. In this case, the laser radiation intensity will be equal to its peak value $G(t)=G_0f_\ell(t)\equiv G_0$, thus allowing the determination of the lowest possible intensity required for a breakdown to occur.

A. Optical breakdown under unlimited action

The classical frequency dependence of the intensity has the form $G^*(\omega_\ell)\sim\omega_\ell^2$ and is satisfied in experiments up to about the left-hand boundary of the visible range $\lambda=0.7\ \mu$m, which approximately corresponds to the frequency of a ruby laser with $\omega_l=4.32\times10^{14}$ s^{-1} ($\lambda_l=0.694\ \mu$m, $\hbar\omega_\ell=1.79$ eV). In the visible and ultraviolet ranges, the threshold intensity does not increase as the frequency grows, moreover it appreciably decreases.[8]

In the present work, the criterion of breakdown, in accordance with Refs. 5 and 23, is taken to be a beginning of a steady domination of the frequency of Coulomb collisions ν_{el} over the frequency of electron-neutral collisions ν_{en}, i.e., $\nu_{\mathrm{ei}}>\nu_{\mathrm{en}}$. The radiation intensity, at which this inequality is satisfied, is taken to be the threshold intensity $G^*(\omega_\ell)$.

In Fig. 2(a), we compare two frequency dependences of the threshold intensity calculated for the case of unlimited duration of action. Curve 1 is close to the classical dependence $G^*(\omega_\ell)$. It corresponds to the solution of the mathematical model in which all the photoprocesses are omitted and only collisional transitions and spontaneous decay of excited states are taken into account. Curve 2 is obtained from the solution of the complete mathematical models (1)–(6), which takes into account all the photoprocesses and collisional reactions. The curves coincide in the IR region only. In the remaining part of the frequency range, Curve 2 is below Curve 1 and has a number of sharp troughs corresponding to the consecutive excitation of electron transitions. The obtained disposition of Curves 1 and 2 indicates a qualitative difference in the behavior of optical breakdown in the IR and UV regions.

Let us analyze and estimate the relative role of collisional reactions and photoprocesses in the development of an electron-ion avalanche in the whole frequency range under consideration. Collisional population of excited states results from inelastic collisions of electrons with atoms and ions. Direct transitions from the ground state, transitions between close levels and transitions from the continuum (triple recombination) contribute to the population of each level. Collisional destruction of excited states occurs due to the processes of ionization and deexcitation by superelastic collisions of the second order.

B. IR-region

As it was shown by mathematical modeling,[5,6] total domination of collisional reactions in the process of optical breakdown occurs in the IR region of frequencies $\hbar\omega_\ell \in [0.12-1.17]$eV, whose boundaries correspond to the CO_2 and Nd–YAG lasers radiation. The main mechanism of developing of an electron-ion avalanche in the IR region is the stepwise ionization. The threshold value $G^*(\omega_\ell)$ for the CO_2 laser operating in the regime of unlimited duration is $G^*(\omega_\ell)=6.5\times10^5$ W/cm^2, the time taken for a breakdown to develop is $\tau^*=10^{-3}$ s. Accordingly, for the Nd–YAG-laser, these values are $G^*(\omega_\ell)=6\times10^7$ W/cm^2, $\tau^*=1.05\times10^{-3}$ s.

The breakdown process proceeds under the conditions of a strong thermodynamical nonequilibrium that is characterized by the following relations:

$$T_e \gg T_g, \quad N_e^{\mathrm{Saha}}(T_g) < N_e < N_e^{\mathrm{Saha}}(T_e), \quad \nu_{\mathrm{ei}} \sim \nu_{\mathrm{en}}.$$

After the optical breakdown stage ended, the system as a whole comes in the course of time to a stationary thermodynamical equilibrium plasma state for which the following relations are satisfied:

$$T_e \approx T_g, \quad N_e = N_i \approx N_e^{\mathrm{Saha}}(T_g) \approx N_e^{\mathrm{Saha}}(T_e), \quad \nu_{\mathrm{ei}} \gg \nu_{\mathrm{en}}.$$

C. UV-region

As the frequency increases, the energy of radiation quanta and the role of photoprocesses grow. Photopopulation and photodestruction of excited states become noticeable when the laser quantum energy becomes comparable to the transition energy ΔE_{mn} or the ionization energy J_n. Photopopulation results from two processes: (1) Selective and nonresonant photoexcitation of the broadened levels by laser radiation and (2) thermal photoexcitation by the continuous spectrum radiation as well as under the action of photorecombination initiated by laser radiation and continuous spectrum radiation. Photodestruction occurs due to spontaneous radiation transitions and photoionization in the laser field and continuous spectrum radiation.

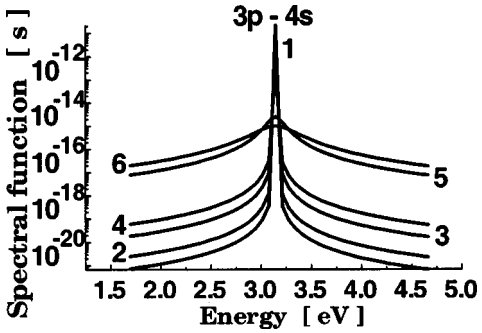

FIG. 3. Spectral function $S(\omega)$ of the resonance transition $3p-4s$ at different time instants: $1-t=10^{-14}$-10^{-12} s; 2-10^{-11} s; 3-10^{-10} s; 4-3$\times10^{-10}$ s; 5-10^{-9} s; and 6-10^{-8} s.

Besides, the collision reactions and photoprocesses may have different directions. Some processes, such as collision excitation by electron impact and photoexcitation are mutually complementary. Others, such as photoionization and ionization by electron impact, are competitive. Thus, the upper excited states are depopulated by collision ionization, in which, as the principal quantum number n grows, the ionization energy decreases as $J_n \sim n^{-2}$. For the low levels $n \leqslant 5$, the photoionization process, whose cross section decreases as $\sigma \sim n^{-5}$ with growing n, is more efficient.

The energy balance of the system in the UV region as a whole is characterized by the following correlations. The laser radiation energy is utilized in the photoexcitation of discrete levels and photoionization heating of free electrons. The energy of free electrons, in addition to photoionization heating, is replenished from the energy of superelastic collisions of excited atoms with the electrons (the extinction reaction). A part of the energy of free electrons is utilized in collision-induced populating of the levels and their subsequent emptying due to ionization. The second part of the energy is transferred via elastic collisions into the translational energy of the atom-ion subsystem. As a result of a complicated energy exchange between different subsystems the optical breakdown in the UV region proceeds, just as in the IR region, under the conditions of a strong nonequilibrium.

As it was shown by calculations, the most obvious influence on the breakdown process as a whole is exerted by the reaction of photoexcitation (selective and nonresonant) and photoionization in the laser field. The interaction of these processes has a competitive character. In order to reveal the influence of each mentioned reaction let us consider in turn the situations in which one of the processes is missing.

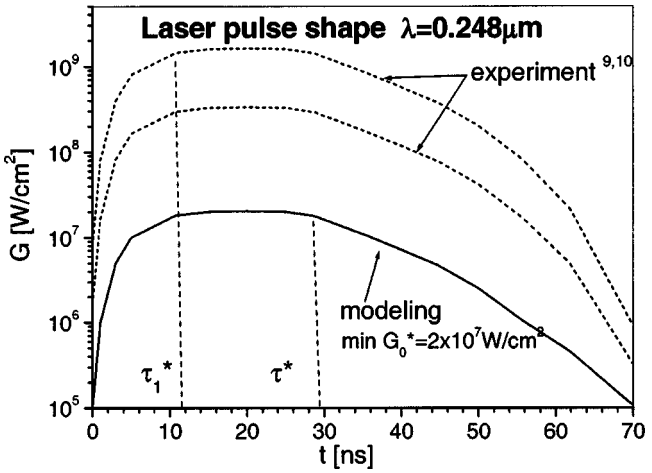

FIG. 4. Temporal dependence of the laser-pulse intensity for the experiments of Refs. 9 and 10. $\tau^*=30$ ns and $\tau_1^*=12$ ns refer to the numerically predicted optical breakdown period for the intensity $G_0=2\times10^7$ W/cm^2 and $G_0=1.6\times10^9$ W/cm^2, respectively.

1. Photoionization

Laser photoionization takes place due to quantum processes. As the frequency ω_ℓ grows, one might expect its role to be continuously enhancing. As long as the energy of the quantum $\hbar\omega_\ell$ is not high, it is only the upper levels that are emptied due to photoionization. Accordingly, their contribution into the general process of ionization is not large. As $\hbar\omega_\ell$ grows, progressively deeper levels are involved into photoionization and one might expect $G^*(\omega_\ell)$ to decrease considerably. But this is not the case. The photoionization process, just as the photoexcitation, is characterized by a noticeable selectivity that is explained by a strong dependence of the photoionization cross-section σ_ϕ on the frequency and the principal quantum number n, $\sigma_\phi\sim n^{-5}$. Therefore, it is the low levels that are depopulated more efficiently due to photoionization, because these levels have the largest cross sections and the highest populations. Figure 2(b) represents the frequency dependence of the threshold sensitivity $G^*(\omega_\ell)$, Curve 3, that is calculated by the model, taking into account the photoionization only and disregarding other photoprocesses. The dependence $G^*(\omega_\ell)$ has a nonmonotonic character and is positioned below Curve 1 corresponding to the classical dependence. The fact that the photoexcitation processes (selective and nonresonant) are excluded from consideration leads to the disappearance of all the sharp troughs in the curve that are due to the excitation of discrete levels and the formation of two noticeable minima. The minima correspond to the energy of atom ionization from the ground state ($J_0=5.98$ eV) and the first excited state ($J_1=2.84$ eV) and are equal to $G^*(\omega_\ell)=10^4$ W/cm^2 and $G^*(\omega_\ell)=2\times10^7$ W/cm^2, respectively. Since before the beginning of breakdown the ground state has the highest population, the minimum in the region of ionization potential J_0 in the frequency dependence $G^*(\omega_\ell)$ has the shape of a sharp trough. Thus, in the UV region, the photoionization in the laser field under the conditions of unlimited laser action turns out to be a strong factor causing the threshold intensity to be reduced by 1.5–2 orders. The one exception is photoionization from the ground state where the reduction of the threshold intensity may be as high as 5–6 orders.

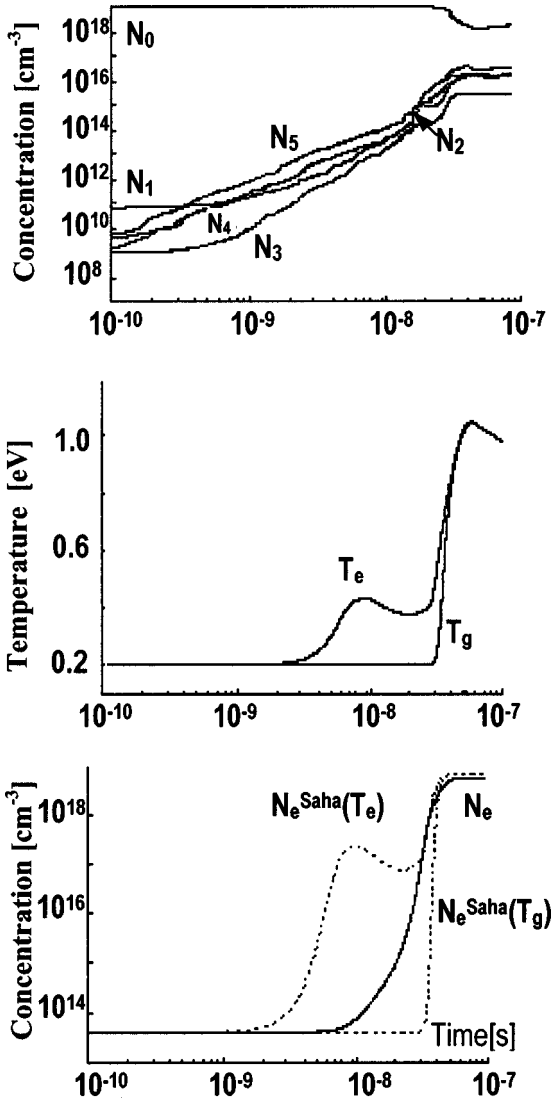

FIG. 5. Temporal dependences of the excited states N_n, the electron density N_e and the temperatures T_e and T_g under the laser action with $\lambda_l=0.248$ μm and $\tau_l=60$ ns.

2. Selective photoexcitation

Selective photoexcitation of discrete levels plays an extremely important role. When selective photoexcitation is taken into consideration with the equal frequencies of the electron transition (coupled–coupled) ω_{mn}^0 and the laser field ω_ℓ, $\omega_{mn}^0=\omega_\ell$, a number of deep and narrow vertical troughs appears in the frequency dependence $G^*(\omega_\ell)$, Fig. 2(c), Curve 4. The resonance excitation of the first four transitions exerts the greatest influence. Thus, the resonance excitation of the first level causes the threshold intensity to be reduced down to 10^2 W/cm^2, i.e., about one order greater than the contribution of the ground-state photoionization. The efficiency of photoexcitation of the second and third levels is comparable to the results of the photoionization of atoms from the ground state. This great influence of the resonance photoionization is explained by the large value of the

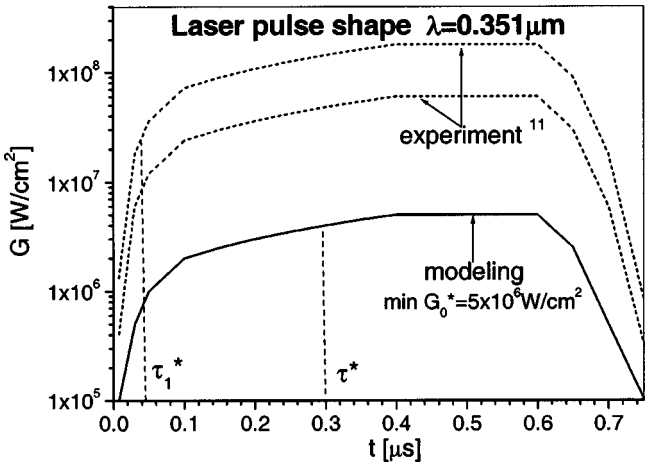

FIG. 6. Temporal dependence of the laser-pulse intensity for the experiments of Ref. 11. $\tau^*=300$ ns and $\tau_1^*=45$ ns refer to the numerically predicted optical breakdown period for the intensity $G_0=5\times10^6$ W/cm^2 and $G_0=1.8\times10^8$ W/cm^2, respectively.

cross-section $\sigma_{mn}(\omega)\sim10^{-12}$ s, that exceeds the photoionization cross section by 5–6 orders and, in accordance with the curve for $G^*(\omega_\ell)$, under the condition of unlimited action can cause the threshold intensity to be reduced by 4–6 orders.

3. Nonresonance photoexcitation

In the absence of an exact resonance between the frequencies of coupled–coupled transitions ω_{mn}^0 and the laser radiation frequency ω_ℓ, $\omega_{mn}^0\neq\omega_\ell$, the laser radiation, regardless of a high degree of monochromaticity due to the presence of the spectral function $S_{mn}(\Delta\omega)$, can be absorbed appreciably in the line wings. As an example of typical broadening of all the transitions, Fig. 3 shows the dynamics of the spectral function $S_{01}(\Delta\omega)$ for the $3p-4s$ transition, giving an impression of the behavior of the line under the combined action of the broadening mechanisms. The line broadening effect underlies the nonresonant populating of the excited state by the laser radiation. The combined influence of the resonance and nonresonance photoexcitations on the frequency dependence $G^*(\omega_\ell)$ is represented in Fig. 2(a), Curve 2. Taking this influence into account in the visible range makes the threshold intensity 2–10 times lower. In the UV range, the influence of photoexcitation sharply increases. The threshold intensity reduces by several orders.

The contribution of the photoprocesses from the continuous spectrum radiation turned out to be insignificant owing to relatively low temperatures of the medium that are characteristic of optical breakdown.

The role of photoionization of the plasma formation process has already been noted,[11,12] but the influence of photoexcitation has not been studied in details. Comparison of the frequency dependences $G^*(\omega_I)$, obtained with allowance for ionization only, Fig. 2(b), Curve 3, and with allowance for all kinds of photoexcitation, Fig. 2(a), Curve 2, shows that in optical breakdown in metal vapors by ultraviolet radiation photoexcitation can play a decisive role, exceeding the contribution of pure photoionization.

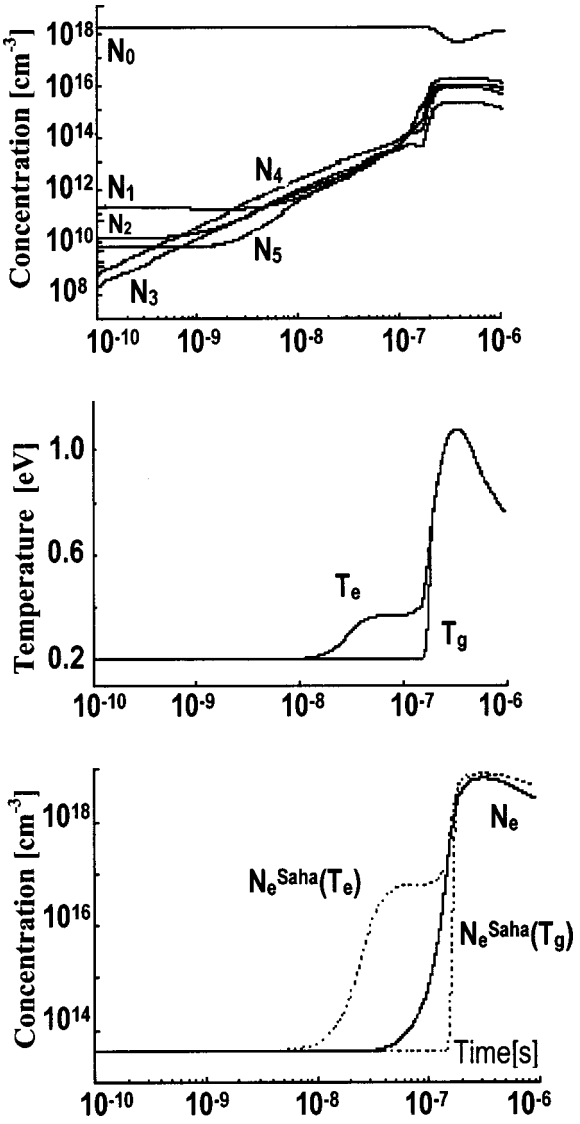

FIG. 7. Temporal dependences of the excited states N_n, the electron density N_e, and the temperatures T_e and T_g under the laser action $\lambda_l=0.355$ μm and $\tau_l=0.75$ μs.

IV. COMPARISON WITH EXPERIMENT

Comparison of modeling results with experimental data serves as a major criterion of the validity of the applied theoretical approach. The models (1)–(6) were used to study several action regimes close to certain experimental situations, where optical breakdown in aluminum vapor by laser radiation pulse was studied.[9–11] The pulses had different duration, temporal shapes and wavelengths. The effects associated with a finite duration of the action and the temporal shape of the laser pulse play a significant role and are to be taken into account.

In the experiments under consideration,[9–11] we note that the plasma formation near the target is always preceded by an intensive evaporation, and the optical breakdown is initiated just in the evaporated matter, but not in the environment gas. In the calculations, the stage of the target heating and evaporation is not considered explicitly but is modeled by giving the initial data corresponding to the parameters of intense evaporation of aluminum

$T_0=0.2$ eV, $N_0^0=\rho_0/M_A=6\times10^{18}$ cm^{-3},

$N_e^0=3\times10_{14}$ cm^{-3}.

Thereby, in mathematical modeling the onset of the laser action turns out to be shifted forward by a time interval required for the heating and establishing of the intense evaporation stage. When comparing the theoretical results with the experimental ones this shift must be taken into account, therefore the situations, where the calculated values of the threshold intensity and the time required for a plasma to be formed did not exceed the experimental data, were taken to be in quite satisfactory agreement.

In experimental situations with pulsed action of excimer lasers on an aluminum target,[9–11] laser pulses had different wavelengths: $\lambda_l=0.248$, 0.355 μm, and different action duration: $\tau_l=60$ ns, 0.75 μs.

A. Experiment 1

The action of the pulsed radiation of the KrF-laser ($\hbar\omega_l=4.99$ eV, $\lambda_l=0.248$ μm) of nanosecond duration on an aluminum target was investigated experimentally in Refs. 9 and 10. The laser pulse of 60 ns duration had a trapezium-like shape with the leading edge of 10 ns, the trailing edge of 15 ns, and the width at the half maximum of 30 ns, Fig. 4. The pulse intensity varied within the range $G_0=(0.33-1.6)\times10^9$ W/cm^2. In the experiments, the complicated structure of the gas dynamic flow was determined, whose constituents were the expanding plasma in the evaporated material and the shock wave in the air.

Mathematical modeling with the given shape and duration of the pulse showed that the threshold intensity of the radiation was $G_0^*=2\times10^7$ W/cm^2, and the optical breakdown time τ^* did not exceed 30 ns, Fig. 4. Taking into account that there was no energy expenditure at the initial stage of the material heating and evaporating, the results obtained can be considered to be in good agreement with the experiment. The peculiarities of the electron-ion avalanche evolution can be characterized with the help of the level population kinetics N_n, change in the concentration and temperature of free electrons N_e, T_e, Fig. 5. The distribution of the excited states N_n shows that for the laser radiation with $\hbar\omega_l=4.99$ eV, the resonance absorption is not observed, since in the quantum structure of the aluminum atom there are no transitions with the energy $\Delta E_{mn}=\hbar\omega_l$. However, the collision broadening of the $3p-4d$ transition results in efficient laser photoexcitation of the $4d$ level (the N_5 concentration). At the expense of collision redistribution between the excited states $5p-4d$ and $5s-5p$, the N_4, N_6 concentrations of the $5s$, $5p$ levels are increased. At the first stage, photoionization of these levels induces additional photoionization heating of free electrons up to the temperature equal to 0.4 eV. This leads to the enhancement of collision excitation of all the levels, the most important role being played by increasing the N_1, N_3 concentrations. After that, the fast phase of collision ionization of excited states begins and the concentration N_e and the temperature T_e grow fast. At the time of 3×10^{-8} s, the quantities N_e and T_e reach their maximum values: $N_e\approx5\times10^{18}$ cm^{-3}, $T_e\approx1.05$ eV, and this completes the plasma formation stage, Fig. 5.

It should be stressed that $G_0^*=2\times10^7$ W/cm^2 presents the minimum intensity that initiates optical breakdown. Modeling was also performed for the maximum intensity considered in the experiments of Refs. 9 and 10, $G_0=1.6\times10^9$ W/cm^2. In this case, the predicted value of the optical breakdown period is much smaller $\tau_1^*=12$ ns, Fig. 4.

B. Experiment 2

The experimental study[11] considered the influence exerted on an aluminum target by the excimer XeF-laser radiation of a microsecond duration with $\hbar\omega_l=3.5$ eV, $\lambda_l=0.355$ μm, and the maximum intensity $G_0=1.8\times10^8$ W/cm^2. The measured plasma formation intensity was in the range $G_0^*\approx6\times10^7-1.8\times10^8$ W/cm^2. The plasma formation time was: $\tau_{\text{exp}}^*=300$ ns at $G_0^*=8\times10^7$ W/cm^2, and $\tau_{\text{exp}}^*=150$ ns at $G_0^*=1.8\times10^8$ W/cm^2. In modeling, the laser-pulse temporal shape was approximated by an asymmetrical trapezium shape with the leading edge of 0.15 μs, the top-hat part of 0.25 μs, and the trailing edge of 0.1 μs, Fig. 6.[11]

Calculations showed that the threshold intensity was $G_0^*=5\times10^6$ W/cm^2, and the break down time was τ^* 300 ns, Fig. 6. The evolution of the main processes is presented in Fig. 7. A distinctive feature of the given interaction is the fact that in the quantum structure of the aluminum atom there is only one transition $3p-4s$, whose energy $\Delta E_{01}=3.14$ eV is close to that of the laser radiation quantum $\hbar\omega_l=3.5$ eV. Owing to collision broadening, the given level is intensively photopopulated by the laser radiation (the concentration N_1). Due to collision redistribution, the excitation is transfered to the $4p$ level, which leads to a considerable increase in the concentration N_3. Because of a relatively large energy difference $\hbar\omega_l-\Delta E_{01}=0.36$ eV the photoexcitation of the $4s$ level has a comparatively moderate rate and in the course of time, the photoionization of this level becomes noticeable. Nevertheless, ultimately, the level population is much greater than the Boltzmann distribution and, hence, differs from it significantly. Other excited states are ionized as a result of collisions with electrons. The plasma formation is completed by the time $t=300$ ns with the parameters $N_e=5\times10^{18}$ cm^{-3}, $T_e=1.07$ eV. The predicted optical breakdown period for the maximum laser intensity of the experiments,[11] $G_0=1.8\times10^8$ W/cm^2, is much shorter $\tau_1^*=45$ ns, Fig. 6.

Thus, in the cases of different action duration and different wavelengths, mathematical modeling demonstrated promising results. In the nanosecond and microsecond ranges of the laser action, the values of the threshold intensity were found to be several times lower than the experimental ones, and the breakdown time τ^* was found to be shorter than the laser-pulse duration $\tau^*<\tau_l$. Taking into account that the initial stage was given approximately, the results obtained seem to possess a sufficient resource in intensity and duration of the laser action for the initial heating and evaporation of the target to be taken into account correctly. Mathematical modeling also showed that development of optical breakdown in the UV region proceeds in a much more complicated way than it does in the IR region. Calculations

showed that for the two wavelengths, the decisive role in the interaction of the laser radiation with aluminum atoms is played by reactions of nonresonance photoexcitation and photoionization.

V. CONCLUSION

The transient collision-radiation model was developed for optical breakdown of a metal vapor with allowance for nonequilibrium laser heating, stepwise collision ionization, and photoprocesses in the laser radiation field and the continuum: photoionization, resonance, and nonresonance photoexcitation of atoms.

Based on the kinetic model, theoretical dependence of optical breakdown in aluminum vapor on the frequency of the radiation threshold intensity $G^*(\omega_\ell)$ was specified. This dependence differs significantly from the classical one and agrees qualitatively with the experimental data.

The main mechanisms of nonequilibrium ionization in the ultraviolet range were determined and analyzed. The modeling showed that in the UV spectrum the development of the electron-ion avalanche proceeds in a much more complicated way as compared to the IR region. In the UV region, the energy quanta of the laser radiation become comparable to the excitation energy of the levels and the ionization potentials of the excited states, thus predetermining the dominant role of the photoprocesses.

The contribution of each photoprocess was analyzed. Resonance photoexcitation leads to the greatest reduction by 5–6 orders of the threshold intensity, but its contribution is significant only in the case when the transition energy exactly coincides with the laser quantum energy $\Delta E_{mn} = \hbar\omega_\ell$. Nonresonance photoexcitation is based on collision broadening of the levels and is described by the spectral function $S(\Delta\omega)$. When it is taken into consideration, the threshold intensity is reduced by 3–4 orders. Since in metal atoms the electron excitation levels are close to each other, the effect of nonresonance photoexcitation acts in a wide spectrum range. Photoionization of the excited states results in reduction of the threshold intensity by 1–2 orders, except photoionization of the ground state $(\hbar\omega_\ell = J_0)$, when the photoionization contribution becomes comparable with the resonance photoexcitation.

The modeling results are in good agreement with the experimental data on optical breakdown in aluminum vapor by excimer laser radiation with λ_l equal to 0.248 and 0.355 μm in the nanosecond and microsecond ranges. The simulated values of the threshold intensity were found to be several times lower than the experimental ones, and the breakdown time was found to be shorter than the laser-pulse duration. This result, along with the fact that the stages of heating and evaporation of the target were disregarded in the calculations, creates prerequisites for a more exact agreement of the results in the case of including the initial stages of the process into consideration.

A complete description of the laser action on condensed media can be accomplished only in the framework of a conjugated problem, in which the elaborated kinetic model will be a constituent of the total mathematical model.

ACKNOWLEDGMENT

The research has been supported by RFBR (Grant No. 01-02-00604)

[1] W. W. Duley, *UV Lasers: Effects and Applications in Materials Science* (University Press, Cambridge, 1996).
[2] M. Humphries, H. J. Kahbert, and K. Pippert, in *Laser in Manufacture*, edited by M. M. Steen (Springer, London, 1987), p. 200.
[3] L. Berthe, R. Fabbro, P. Peyre, and E. Bartnicki, J. Appl. Phys. **85**, 7552 (1999).
[4] R. Fabbro, P. Peyre, L. Berthe, A. Sollier, and E. Bartnicki, Proc. SPIE **3888**, 155 (2000).
[5] V. I. Mazhukin, I. V. Gusev, I. Smurov, and G. Flamant, Microchem. J. **50**, 413 (1994).
[6] V. I. Mazhukin, V. V. Nossov, I. Smurov, and G. Flamant, Surv. Math. Ind. **10**, 45 (2001).
[7] Ya. B. Zeldovich and Yu. P. Raizer, *Physics of Shock Waves and High Temperature Hydrodynamics Phenomena I* (Academic, New York, 1967).
[8] Yu. P. Raizer, *Physics of Gas Discharge* (Nauka, Moskva, 1987).
[9] H. Schittenhelm, G. Callies, P. Berger, and H. Hugel, J. Phys. D **29**, 1564 (1996).
[10] H. Schittenhelm, G. Callies, P. Berger, and H. Hügel, Appl. Surf. Sci. **109/110**, 494 (1997).
[11] D. I. Rosen, J. Mitteldorf, G. Kothandaraman, A. N. Pirri, and E. R. Pugh, J. Appl. Phys. **53**, 3190 (1982).
[12] V. P. Ageev, A. A. Gorbunov, V. I. Konov, D. S. Lukovnikov, S. V. Melchenkov, A. M. Prokhorov, and V. F. Tarasenko, Kvant. Elektron. (Moscow) **10**, 1466 (1983) [Quantum Electron. **13**, 954 (1983)].
[13] V. P. Ageev, A. A. Gorbunov, V. P. Danilov, V. I. Konov, and P. I. Nikitin, Kvant. Elektron. (Moscow) **10**, 2451 (1983) [Quantum Electron. **13**, 1595 (1983)].
[14] E. O. Danilov, V. A. Danilichev, V. A. Dolgikh, V. D. Zvorikin, M. E. Zemskov, O. M. Kerimov, G. E. Metreveli, and G. Yu. Tamanyan, Kvant. Elektron. (Moscow) **10**, 2560 (1988) [Quantum Electron. **18**, 1610 (1988)].
[15] E. O. Danilov, V. A. Danilichev, V. A. Dolgikh, V. D. Zvorikin, M. E. Zemskov, O. M. Kerimov, G. E. Metreveli, and G. Yu. Tamanyan, Kvant. Elektron. (Moscow) **15**, 2568 (1988) [Quantum Electron. **18**, 1615 (1988)].
[16] G. M. Weyl and D. I. Rosen, Phys. Rev. A **31**, 2300 (1985).
[17] K. Kadawa, S. Yokoi, and S. Nakajima, Opt. Commun. **45**, 261 (1983).
[18] G. Weyl, A. Pirri, and R. Root, AIAA J. **10**, 460 (1981).
[19] D. I. Rosen, D. E. Hastings, and G. M. Weyl, J. Appl. Phys. **53**, 5882 (1982).
[20] A. N. Pirri, R. G. Root, and P. K. S. Wu, AIAA J. **16**, 1296 (1978).
[21] A. M. Popov, Zh. Tekh. Fiz. **52**, 2105 (1982) [Tech. Phys. **27**, 1352 (1982)].
[22] M. Ignatavichus, E. Kazakiavichus, G. Orshevsky, and V. Danunas, Kvant. Elektron. (Moscow) **18**, 1325 (1991) [Quantum Electron. **21**, 1210 (1991)].
[23] M. Mitchner and C. H. Kruger, *Partially Ionized Gases* (Wiley, New York, 1973).
[24] W. J. Wiese, M. W. Smith, and B. M. Miles, *Transition Probabilities*, Vol. **2** (NBS, Washington, 1969).
[25] C. W. Allen, *Astrophysical Quantities* (Athlone Press, University of London, 1973).
[26] H. Van Regemorter, Astrophys. J. **132**, 906 (1962).
[27] R. Mewe, Astron. Astrophys. **20**, 256 (1972).
[28] W. Lotz, Z. Phys. **232**, 101 (1970).
[29] W. Lotz, Astrophys. J., Suppl. **14**, 207 (1967).
[30] A. Burgess and M. J. Seaton, Rev. Mod. Phys. **30**, 992 (1958).
[31] A. Burgess and M. J. Seaton, Mon. Not. R. Astron. Soc. **120**, 121 (1960).
[32] V. I. Derzhiev, A. G. Zhidkov, and S. I. Yakovlenko, *Radiation of Ions in Dense Non-equilibrium Plasma* (Energoatomizdat, Moskva, 1986).
[33] S. I. Yakovlenko, *Collision-Radiative Phenomena* (Energoatomizdat, Moskva, 1984).
[34] H. R. Griem, *Plasma Spectroscopy* (McCraw-Hill, New York, 1964).
[35] L. A. Vainshtein, I. I. Sobelman, and E. A. Yukov, *Excitation of Atoms and Spectral Line Broadening* (Nauka, Moskva, 1979).
[36] *Reactions under plasma conditions*, Vol. **1**, edited by M. Venugopalan (Wiley, New York, 1971).
[37] V. Weisskopf, Zs. Phys. **75**, 287 (1932).

[38] G. Traving, in *Plasma Diagnostics*, edited by W. Lochte-Holtgreven (North-Holland, Amsterdam, 1968), p. 57.
[39] L. M. Biberman and G. E. Norman, Usp. Fiz. Nauk **91**, 193 (1967) [Phys. Usp. **10**, 52 (1967)].
[40] C. W. Gear, J. Comput. Math. **21**, 146 (1967).
[41] C. D. Byrne and A. C. Hindmarsh, J. Comput. Phys. **70**, 1 (1987).
[42] E. Hairer, S. P. Norsett, and G. Wanner, *Solving Ordinary Differential Equation. Part I: Non-stiff Problems* (Springer-Verlag, Berlin, 1989).
[43] E. Hairer, S. P. Norsett, and G. Wanner, *Solving Ordinary Differential Equation. Part II: Stiff Problems* (Springer-Verlag, Berlin, 1991).
[44] C. W. Gear, J. Assoc. Comput. Mach. **14**, 185 (1965).
[45] A. C. Hindmarsh, and C. D. Byrne, in *Numerical Methods for Differential Systems*, edited by L. Lapidus and W. E. Schiesser (Academic Press, New York, 1976), p. 147.
[46] A. C. Hindmarsh, ACM-SIGNUM Newsletter **15**, 10 (1980).
[47] C. J. Knight, AIAA J. **17**, 519 (1979).